EIT image reconstruction based on a hybrid FE-EFG forward method and the complete-electrode model

M. Hadinia[1], R. Jafari[1] and M. Soleimani[2]

[1]Faculty of Electrical Engineering, K. N. Toosi University of Technology, Tehran, Iran
[2]Engineering Tomography Lab (ETL), Electronic and Electrical Engineering, University of Bath, Bath, UK.
Email: m_hadinia@ee.kntu.ac.ir, jafari@eetd.kntu.ac.ir, m.soleimani@bath.ac.uk.

Abstract- This paper presents the application of the hybrid finite element- element free Galerkin (FE-EFG) method for the forward and inverse problems of electrical impedance tomography (EIT). The proposed method is based on the complete electrode model. Finite element (FE) and element free Galerkin (EFG) methods are accurate numerical techniques. However, FE technique has meshing task problems and EFG method is computationally expensive. In this paper, the hybrid FE-EFG method is applied to take both advantages of FE and EFG methods, the complete electrode model of the forward problem is solved, and an iterative regularized Gauss–Newton method is adopted to solve the inverse problem. The proposed method is applied to compute Jacobian in the inverse problem. Utilizing two dimensional circular homogenous models, the numerical results are validated with analytical and experimental results and the performance of the hybrid FE-EFG method compared with the FE method is illustrated. Results of image reconstruction are presented for a human chest experimental phantom.

Keywords- electrical impedance tomography, forward problem, inverse problem, complete electrode model, element free Galerkin method, finite element method, hybrid finite element- element free Galerkin method.

1. Introduction

Electrical impedance tomography (EIT) is an imaging technique with existing and potential applications in engineering and medical problems. In this method, electric currents are injected into a conductive object through electrodes placed on its surface, and the resulting electric potential on the electrodes is determined. Injecting currents in different patterns, a finite number of boundary measurements are taken (Cheney *et al* 1999, Saulnier *et al* 2001).

Image reconstruction in EIT includes forward and inverse problems. In the inverse problem, using the measured and modeled data, the internal resistivity profile is estimated by minimizing a cost function in an iterative procedure.

The EIT forward problem provides modeled data for comparing with experimental data in the inverse problem. The ability of the forward model to produce the corresponding data efficiently plays a key role in the EIT. The first step in the EIT forward problem is to make a physical model called forward model that calculates the voltages on the surface with given applied currents and conductivity distribution. The potential in the domain of EIT problem can be governed by Laplace equation. The four common boundary conditions, known as EIT electrode models, are the continuum, gap, shunt and complete electrode models (Vauhkonen *et al* 1999, Cheng *et al* 1989*,* Somersalo *et al* 1992, Vauhkonen 1997). The most accurate model that has been presented is the complete electrode model (CEM). In the CEM both the shunting effect of the electrodes and the contact impedances between the electrodes and body are contemplated (Vauhkonen *et al* 1999).

To solve the EIT forward problem various traditional numerical methods including the boundary element (BE) method, the finite element (FE) method, and the mesh free methods have been applied (Ghaderi Daneshmand and Jafari 2013, Muria and Kagwa 1985, Yousefi *et al* 2013).

Some of the literature have used the BE method to solve the EIT forward problem based on the CEM (Xu and Dong 2010). It is hard to solve problems including a large number of heterogeneous subregions with the BE method (Ghaderi Daneshmand and Jafari 2013, Vauhkonen 1997). The FE method is more appropriate for solving EIT forward problems with non-homogeneous conductivity distributions on irregular domains. The FE method requires discretization of the entire region into elements in a FE mesh. FE mesh generation and data pre-processing sometimes are difficult and time-consuming, especially for three-dimensional irregular objects with complex internal structure like heterogeneous biological tissues in the human head models. For instance, a human head model was discretized into 155915 elements in the literature (Bayford *et al* 2001). Furthermore, the traditional FE method uses node connectivity or elements so the solution of the FE method can be affected by the

quality of a mesh, but mesh construction cannot always be completely automated (Šterk and Trobec 2008). Some of the literatures have employed the FE method to solve the EIT forward problems based on the CEM (Vauhkonen *et al* 1999).

Being able to obtain the solution of forward problem in EIT using meshfree methods would have the advantage of eliminating the element connectivity requirement of the FE method. In the literature, a number of meshfree methods have recently been introduced (Belytschko *et al* 1994, Dolbow and Belytschko 1998, Hegen 1996, Hkrault and Markcha1 1999, Šterk and Trobec 2008, Yousefi *et al* 2014,). Among meshfree methods, element free Galerkin (EFG) method, which is based on moving least squares approximation (MLSA), is a well-known numerical method used for solving boundary value problems. In (Gang *et al* 2013), a meshless local Petrov-Galerkin (MLPG) method is used in the EIT forward problem based on a simple electrode model. In (Hadinia and Jafari 2015) the EFG method is used for solving forward problem based on the CEM. Since a linear system has to be solved for each point of the problem domain, the MLSA is computationally expensive. Furthermore, a dense integration pattern is necessary to get accurate values for the resulting linear system (Hegen 1996). Additionally, in the EFG method, the imposition of the essential boundary conditions is difficult (Hkrault and Markcha1 1999). On the other hand, the FE method can be more efficient in many cases because of the direct way for assembling the stiffness matrix and its effective treatment of boundary conditions (Cutrupi *et al* 2007). Therefore, a combination of the EFG method and the FE method can take the advantages of the FE and EFG methods.

In (Hadinia *et al* 2015) a combination of the EFG method and the FE method is used for solving the EIT forward problem based on the CEM.

Different techniques have been used to solve the EIT inverse problems. One of the most commonly used methods in the EIT inverse problem, is Gauss–Newton or modified Newton–Raphson method (Yorkey *et al* 1987). In (Cutrupi *et al* 2007), an approach based on a combination of the EFG and FE methods is used in the EIT inverse problem based on a simple electrode model. (Cutrupi *et al* 2007) have assumed the shape and size of inhomogeneity are known and the position of the centre of the inhomogeneity has just been estimated by use of a time-consuming Genetic Algorithm.

In this research work, the hybrid FE-EFG method is applied to solve the EIT forward problem based on the CEM and the Gauss–Newton method has been applied in order to solve the EIT inverse problem within reasonable times. The Gauss–Newton method requires the Jacobian, describing the mapping between voltage distribution on the body's surface and the unknown physical parameter distribution in the interior of body. To compute the elements of Jacobian matrix, the governing equations are solved by the hybrid FE-EFG forward method.

The comparison of electrode voltage solutions obtained from both FE and hybrid FE-EFG methods have been done and validated against the corresponding analytic solution and experimental results for 2D homogenous models. For the inverse problem simulations, the experimental chest phantom presented in (Isaacson *et al* 2004) is considered. The FE and the hybrid FE-EFG solution of CEM are used as forward model, the inverse problem is solved with the Gauss–Newton method, and the results of image reconstruction are demonstrated.

This paper is organized as follows. In Section 2, the mathematical model for the EIT forward problem based on the complete electrode model together with the hybrid FE-EFG numerical method is presented. In Section 3, the EIT inverse problem and the computation of Jacobian in the EIT inverse problem is described. Simulation results are reported in Section 4. Conclusion of paper is presented in Section 5.

2. EIT forward problem

2.1. Governing equations

Consider a two-dimensional (2D) region Ω with conductivity σ and its boundary Γ with L electrodes. The EIT forward problem based on the CEM consists of the following equations (Vauhkonen *et al* 1999, Cheng *et al* 1989, Somersalo *et al* 1992, Vauhkonen 1997)

$$\nabla \cdot \sigma \nabla u = 0 \tag{1}$$

$$u + z_l \sigma \frac{\partial u}{\partial n} = U_l \qquad \text{on } \Gamma_{E_l},\ l = 1,2,\ldots,L \tag{2}$$

$$\int_{\Gamma_{E_l}} \sigma \frac{\partial u}{\partial n} d\Gamma = I_l \tag{3}$$

$$\sigma \frac{\partial u}{\partial n} = 0 \qquad x \in \partial\Omega \setminus \cup_{l=1}^{L} \Gamma_{E_l} \tag{4}$$

where u is the electric potential distribution, n is the outward unit vector which is normal to the boundary, the z_l is effective contact impedance between the l-th electrode and the 2D region, U_l is the measured voltage on the l-th electrode, I_l is the injected current in to l-th electrode, and Γ_{E_l} denotes the l-th electrode. The expression $x \in \partial\Omega \setminus \cup_{l=1}^{L} \Gamma_{E_l}$ indicates the point x is on the boundary and is not under the electrodes.

Additionally, two other conditions are needed in the EIT forward problem based on the CEM. To ensure the existence of a real solution, the first condition that should be satisfied is:

$$\sum_{l=1}^{L} I_l = 0 \tag{5}$$

In order to ensure the uniqueness of the solution, the following condition is also employed:

$$\sum_{l=1}^{L} U_l = 0 \tag{6}$$

In (Somersalo *et al* 1992), it has been shown that the following $B((u,U),(v,V))$ is the equivalent variational problem of the EIT forward problem above:

$$B((u,U),(v,V)) = \int_{\Omega} \sigma \nabla u \cdot \nabla v \, d\Omega + \sum_{l=1}^{L} \frac{1}{z_l} \int_{\Gamma_{E_l}} (u-U)(v-V) \, d\Gamma = \sum_{l=1}^{L} I_l V_l \tag{7}$$

In the proposed hybrid FE-EFG method, the domain Ω should be divided into two regions: an outer region Ω^{FE} near the boundaries and an inner region Ω^{EFG}. The outer and inner regions are formulated by the FE and the EFG methods, respectively. Figure 1 depicts the two FE and EFG regions. The regions Ω^{FE} and Ω^{EFG} are adjacent ($\Omega = \Omega^{FE} \cup \Omega^{EFG}$). Γ^{FE} and Γ^{EFG} are the boundaries of Ω^{FE} and Ω^{EFG}, respectively, and Γ^{int} is the interface boundary. Selecting the FE region as outer region is because of the simplicity. In general, depending on the actual case, both EFG and FE regions can be used as boundary region.

The EFG discretization can be used for representing domains that has meshing tasks like moving parts or regions affected by large deformations. Other regions with fix shaped parts and regions that meshing is easy for them can be considered as FE regions. If extremely high-resolved meshes are required in certain parts of the domain, the hybrid FE-EFG approach is advantageous compared to the pure FE method (Cutrupi *et al* 2007).

In (Hadinia *et al* 2015) the effect of the size of FE and EFG regions on the accuracy of the hybrid FE-EFG method is investigated for an inhomogeneous circular model. Results are shown that the accuracy and the execution time of the hybrid FE-EFG method is increased as the size of EFG region increases.

For discretizing of region in the hybrid method, domains with meshing task problem are considered as EFG region, according to anatomical pre information. Other regions can be considered as FE regions. The size of FE region depends on our preference between more accuracy or less computational time. The smaller FE region leads to increasing the accuracy and moreover increasing the execution time.

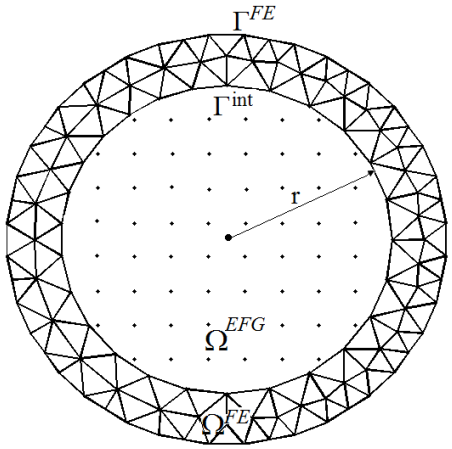

Figure 1. Domain handled by EFG and FE regions

2.2. FE shape functions

In the FE region Ω^{FE}, the domain is divided into M triangular elements and includes N^{FE} nodes. Electrical potential u^{FE} at each point is given by a linear interpolation of nodal value $\hat{u}_i^{FE}$ (Vauhkonen 1997):

$$u^{FE}(\mathbf{x}) = \sum_{i=1}^{N^{FE}} \Phi_i^{FE}(\mathbf{x}) \hat{u}_i^{FE} \quad \forall \mathbf{x} \in \Omega^{FE} \tag{8}$$

where $\mathbf{x}$ is a variable that represents the point (x, y) in the plane of the region Ω^{FE} and $\Phi_i^{FE}(\mathbf{x})$, $(i = 1 : N^{FE})$ are linear nodal shape functions, these shape functions are piecewise polynomial over the elements and have the selectivity property i.e. $\Phi_j(\mathbf{x}_i) = \delta_{ij} = \begin{cases} 1 & i = j \\ 0 & i \neq j \end{cases}$ thus $u^{FE}(\mathbf{x}_i) = \hat{u}_i^{FE}$.

2.3. EFG shape functions

In the EFG region, the domain consists of N^{EFG} nodes. The shape function in the EFG method is determined by means of the MLSA. Then, the following approximation equation for u^{EFG} is adopted (Belytschko *et al* 1994, Dolbow and Belytschko 1998)

$$u^{EFG}(\mathbf{x}) = \sum_{i=1}^{N^{EFG}} \Phi_i^{EFG}(\mathbf{x}) \hat{u}_i^{EFG} \quad \forall \mathbf{x} \in \Omega^{EFG} \tag{9}$$

where $\mathbf{x}$ is a variable that represents the point (x, y) in the plane of the region Ω^{EFG}, $\hat{u}_i^{EFG}$ is the approximation to the value $u^{EFG}(\mathbf{x})$ at the node $\mathbf{x}_i$, and Φ^{EFG} is the shape function for EFG method obtained by means of the MLSA method. To obtain the shape functions through the MLSA, there is a standard technique in the element-free Galerkin approach. The mathematical details can be found in (Belytschko *et al* 1994, Dolbow and Belytschko 1998).

2.4. Hybrid FE-EFG method

In this subsection, the EIT forward problem based on the CEM is formulated. To couple FE and EFG methods, the following continuity conditions have to be enforced on the interface boundary Γ^{int} between the two regions Ω^{FE} and Ω^{EFG}:

$$u^{FE}(\mathbf{x}) = u^{EFG}(\mathbf{x}) \quad \mathbf{x} \in \Gamma^{\text{int}} \tag{10}$$

$$\sigma \nabla u^{FE}(\mathbf{x}) \cdot \hat{n}^{FE}\big|_{\Gamma^{\text{int}}} = -\sigma \nabla u^{EFG}(\mathbf{x}) \cdot \hat{n}^{EFG}\big|_{\Gamma^{\text{int}}} \tag{11}$$

where $\hat{n}^{FE}$ and $\hat{n}^{EFG}$ are outward unit vectors which are normal to the Γ^{int} in the FE and EFG regions, respectively. To impose (10) and (11) on the interface boundary, consider arbitrary functions $v^{FE}(\mathbf{x})$, $v^{EFG}(\mathbf{x})$, $\gamma(\mathrm{x})$, V. The weak form (7) can then be extended for the FE and EFG regions using a similar variational technique introduced in (Hegen 1996) as follows:

$$\int_{\Omega^{FE}} \sigma \nabla u^{FE} \cdot \nabla v^{FE} \, d\Omega - \int_{\Gamma^{\text{int}}} v^{FE} \lambda \, d\Gamma - \int_{\Gamma^{\text{int}}} u^{FE} \gamma \, d\Gamma + \sum_{l=1}^{L} \frac{1}{z_l} \int_{\Gamma_{E_l}} (u^{FE} - U)(v^{FE} - V) \, d\Gamma = \sum_{l=1}^{L} I_l V|_{on\ \Gamma_{E_l}} \tag{12}$$

and

$$\int_{\Omega^{EFG}} \sigma \nabla u^{EFG} \cdot \nabla v^{EFG} \, d\Omega + \int_{\Gamma^{\text{int}}} v^{EFG} \lambda \, d\Gamma + \int_{\Gamma^{\text{int}}} u^{EFG} \gamma \, d\Gamma = 0 \tag{13}$$

where the function λ is a Lagrange multiplier. To discretize the above equations, the functions U and λ should be discretized. The voltage function U on the electrodes is approximated as:

$$U|_{on\ \Gamma_{E_l}} = U_l = \sum_{m=1}^{L-1} n_{l,m} \hat{U}_m \tag{14}$$

where $\hat{U}_m$ are the coefficients to be determined, and constant coefficients $n_{l,m}$ are defined as:

$$n_{l,m} = \begin{cases} 1 & l = 1 \quad m = 1, \cdots, L-1 \\ -1 & 2 \le l \le L \quad m = l - 1 \\ 0 & 2 \le l \le L \quad m \neq l - 1 \end{cases} \tag{15}$$

This selection of coefficients ensures that equation (6) is valid. From equations (14) and (15) the potentials U_l on the electrodes are calculated as:

$$\begin{aligned} U_1 &= \sum_{l=1}^{L-1} \hat{U}_l \\ U_2 &= -\hat{U}_1 \\ &\vdots \\ U_l &= -\hat{U}_{l-1} \\ &\vdots \\ U_L &= -\hat{U}_{L-1}. \end{aligned} \tag{16}$$

The function λ can be expressed as:

$$\lambda(\mathbf{x})|_{\Gamma_{\text{int}}} = \sum_{h=1}^{N_s} N_h(\mathbf{x})\hat{\lambda}_h \tag{17}$$

where

$$N_h(\mathbf{x}) = \delta(\mathbf{x} - \mathbf{x}_{Lh}) \quad \mathbf{x}_{Lh} \in \Gamma^{\text{int}}, \quad h = 1,\ldots,N_s \tag{18}$$

where N_s is the number of common nodes located on Γ^{int} and $\delta(\mathbf{x})$ is the Dirac delta function.

Substituting (8), (14), and (17) into (12) and (9) and (17) into (13), and letting $v^{FE} = \Phi_i^{FE}$, $v^{EFG} = \Phi_i^{EFG}$, $\gamma = \delta(\mathbf{x} - \mathbf{x}_{Lh})$ and $V = n_{l,m}$ yield the following linear system for $\hat{\mathbf{u}}^{FE}$, $\hat{\mathbf{u}}^{EFG}$, $\hat{\mathbf{U}}$, and $\hat{\boldsymbol{\lambda}}$, the vectors which are made up of $\hat{u}_i^{FE}$, $\hat{u}_i^{EFG}$, $\hat{U}_m$, and $\hat{\lambda}_h$, respectively:

$$\mathbf{A}_{n\times n}\mathbf{b}_{n\times 1} = \mathbf{F}_{n\times 1} \tag{19}$$

Where n is the number of unknowns ($n = N^{FE} + N^{EFG} + L - 1 + N_s$), $\mathbf{b} = \begin{bmatrix} \hat{\mathbf{u}}^{FE} & \hat{\mathbf{u}}^{EFG} & \hat{\mathbf{U}} & \hat{\boldsymbol{\lambda}} \end{bmatrix}^T$, $\mathbf{F} = \begin{bmatrix} \mathbf{0} & \tilde{\mathbf{I}} & \mathbf{0} & \mathbf{0} \end{bmatrix}^T$, and

$$\mathbf{A} = \begin{bmatrix} \mathbf{B}^{FE} & \mathbf{0} & \mathbf{C}^{FE} & \mathbf{G}^{FE} \\ \mathbf{C}^{FE} & \mathbf{0} & \mathbf{D}^{FE} & \mathbf{0} \\ \mathbf{0} & \mathbf{K}^{EFG} & \mathbf{0} & \mathbf{G}^{EFG} \\ \mathbf{G}^{FE} & \mathbf{G}^{EFG} & \mathbf{0} & \mathbf{0} \end{bmatrix} \tag{20}$$

The elements of matrices $\mathbf{B}^{FE}$, $\mathbf{C}^{FE}$, $\mathbf{D}^{FE}$, $\mathbf{K}^{EFG}$, $\mathbf{G}^{FE}$ and $\mathbf{G}^{EFG}$ are obtained as follows

$$B_{i,j}^{FE} = \int_{\Omega^{FE}} \sigma \nabla\Phi_i^{FE} \cdot \nabla\Phi_j^{FE} d\Omega + \sum_{l=1}^{L} \frac{1}{z_l} \int_{\Gamma_{E_l}} \Phi_i^{FE}\Phi_j^{FE} d\Gamma \qquad i,j = 1,2,\ldots,N^{FE} \tag{21}$$

$$C_{i,m}^{FE} = -\frac{1}{z_1} \int_{\Gamma_{E_1}} \Phi_i^{FE} d\Gamma + \frac{1}{z_{m+1}} \int_{\Gamma_{E_{m+1}}} \Phi_i^{FE} d\Gamma \qquad i = 1,2,\ldots,N^{FE} \quad m = 1,2,\ldots,L-1 \tag{22}$$

$$D_{k,m}^{FE} = \sum_{l=1}^{L} \frac{1}{z_l} \int_{\Gamma_{E_l}} n_{l,k}\, n_{l,m}\, d\Gamma = \begin{cases} \dfrac{e_1}{z_1}, & k \neq m \\ \dfrac{e_1}{z_1} + \dfrac{e_{m+1}}{z_{m+1}}, & k = m \end{cases}, \quad k,m = 1,2,\ldots,L-1 \tag{23}$$

$$K_{i,j}^{EFG} = \int_{\Omega^{EFG}} \sigma \nabla\Phi_i^{EFG} \cdot \nabla\Phi_j^{EFG} d\Omega \qquad i,j = 1,2,\ldots,N^{EFG} \tag{24}$$

$$G_{i,h}^{FE} = \begin{cases} -1 & \mathbf{x}_i = \mathbf{x}_{Lh} \\ 0 & \mathbf{x}_i \neq \mathbf{x}_{Lh} \end{cases} \quad i = 1,2,\ldots,N^{FE}, \quad \mathbf{x}_{Lh} \in \Gamma^{\text{int}}, \quad h = 1,\ldots,N_s \tag{25}$$

$$G_{i,h}^{EFG} = \Phi_i^{EFG}(\mathbf{x}_{Lh}) \quad i = 1,2,\ldots,N^{EFG}, \quad \mathbf{x}_{Lh} \in \Gamma^{\text{int}}, \quad h = 1,\ldots,N_s \tag{26}$$

where e_m is the length of the m-th electrode in 2D. The expanded matrix forms of $\widetilde{\mathbf{I}}$, $\mathbf{G}^{FE}$ and $\mathbf{G}^{EFG}$ are written as follows:

$$\widetilde{\mathbf{I}} = \begin{bmatrix} (I_1 - I_2) & (I_1 - I_3) & \dots & (I_1 - I_L) \end{bmatrix}^T \tag{27}$$

$$\mathbf{G}^{FE\,T} = \begin{bmatrix} 0 & \dots & -1|_{1,i} & 0 \\ \vdots & & \ddots & \vdots \\ 0 & \dots & -1|_{N_s,i} & 0 \end{bmatrix}_{N_s \times N^{FE}} \tag{28}$$

$$\mathbf{G}^{EFG\,T} = \begin{bmatrix} \Phi_1^{EFG}(\mathbf{x}_{L1}) & \Phi_2^{EFG}(\mathbf{x}_{L1}) & \dots & \Phi_{N^{EFG}}^{EFG}(\mathbf{x}_{L1}) \\ \Phi_1^{EFG}(\mathbf{x}_{L2}) & \Phi_2^{EFG}(\mathbf{x}_{L2}) & \dots & \Phi_{N^{EFG}}^{EFG}(\mathbf{x}_{L2}) \\ \vdots & \vdots & & \vdots \\ \Phi_1^{EFG}(\mathbf{x}_{LN_s}) & \Phi_2^{EFG}(\mathbf{x}_{LN_s}) & \dots & \Phi_{N^{EFG}}^{EFG}(\mathbf{x}_{LN_s}) \end{bmatrix}_{N_s \times N^{EFG}} \tag{29}$$

where i is the global node number in the FE region.

Solving the equation (19) using Gaussian elimination method, $\mathbf{b} = \begin{bmatrix} \hat{\mathbf{u}}^{FE} & \hat{\mathbf{u}}^{EFG} & \hat{\mathbf{U}} & \hat{\boldsymbol{\lambda}} \end{bmatrix}^T$ is obtained.

3. EIT inverse problem

The EIT inverse problem is to determine the distribution of electrical resistivity by minimizing a cost function. The following cost function which is a function of the difference between the measured potentials and the calculated potentials is employed in this paper (Yorkey *et al* 1987):

$$E(\boldsymbol{\rho}) = \frac{1}{2}(\mathbf{f}(\boldsymbol{\rho}) - \mathbf{Vo})^T(\mathbf{f}(\boldsymbol{\rho}) - \mathbf{Vo}) \tag{30}$$

where $\boldsymbol{\rho}$ is the resistivity distribution vector, $\mathbf{Vo}$ is the measured potential vector, and $\mathbf{f}$ is the potential vector obtained from the forward problem. The function E should be minimized to find a point $\boldsymbol{\rho}_n$ which is at least a local minimum. Differentiating the function E' with respect to $\boldsymbol{\rho}$ and set the result equal to zero vector, $\Delta\boldsymbol{\rho}^k$ can be formulated as a system of linear equations as follows (Yorkey *et al* 1987):

$$[\mathbf{f}'(\boldsymbol{\rho}^k)]^T\mathbf{f}'(\boldsymbol{\rho}^k)\Delta\boldsymbol{\rho}^k = -\left[\mathbf{f}'(\boldsymbol{\rho}^k)\right]^T\left(\mathbf{f}(\boldsymbol{\rho}^k) - \mathbf{Vo}\right) \tag{31}$$

where the matrix, $\mathbf{f}'$ is called the Jacobian matrix or sensitivity matrix. The product of the transpose of the Jacobian matrix with itself is called the Hessian matrix, $[\mathbf{f}']^T\mathbf{f}'$, whose its inverse needs to be calculated during every iterative step. Hessian matrix is ill conditioned. Hence small changes in the Hessian data produce a large change in solution of the inverse problem. It is therefore necessary to incorporate some regularization methods. Using the iterative regularized Gauss-Newton method at the iteration k yields (Razmjoo *et al* 2010):

$$\Delta\boldsymbol{\rho}^k = -\left([\mathbf{f}'(\boldsymbol{\rho}^k)]^T\mathbf{f}'(\boldsymbol{\rho}^k) + \mu\mathbf{R}\right)^{-1}\left[\mathbf{f}'(\boldsymbol{\rho}^k)\right]^T\left(\mathbf{f}(\boldsymbol{\rho}^k) - \mathbf{Vo}\right) \tag{32}$$

where $\mathbf{R}$ is a regularization matrix which could be an identity matrix and μ is a control parameter determining the amount of regularization used

Using (32), the resistivity vector $\boldsymbol{\rho}^k$ is updated at k-th iteration as

$$\boldsymbol{\rho}^{k+1} = \boldsymbol{\rho}^k + \Delta\boldsymbol{\rho}^k \tag{33}$$

If the function $E(\boldsymbol{\rho})$ reaches a predetermined fixed value E_0 or iteration index be equal to a predetermined value N_0, the iterative procedure is stopped.

3.1. Computation of Jacobian matrix

In this paper to calculate the Jacobian matrix, the standard method described in (Vauhkonen 1997) is used. Assume, that the domain Ω is discretized with N_s pixels with unknown resistivities to be determined, and the resistivity distribution is piecewise constant. Differentiation of equation (19) with respect to the resistivity of m-th pixel, ρ_m, results to:

$$\frac{\partial(\mathbf{A}\,\mathbf{b})}{\partial\rho_m}=\frac{\partial\mathbf{F}}{\partial\rho_m} \tag{34}$$

Considering $\partial\mathbf{F}/\partial\rho_m$ is equal to zero and expanding the left hand side of (34) give:

$$\frac{\partial\mathbf{A}}{\partial\rho_m}\mathbf{b}+\mathbf{A}\frac{\partial\mathbf{b}}{\partial\rho_m}=0 \tag{35}$$

or

$$\mathbf{A}\frac{\partial\mathbf{b}}{\partial\rho_m}=-\frac{\partial\mathbf{A}}{\partial\rho_m}\mathbf{b}\,. \tag{36}$$

The Gaussian elimination method can be used to solve the resulting linear system of equation (36) for $\partial\mathbf{b}/\partial\rho_m$. Since only the matrixes $\mathbf{B}^{FE}$ and $\mathbf{K}^{EFG}$ in $\mathbf{A}$ depend on ρ the derivative $\partial\mathbf{A}/\partial\rho_m$ can be computed as:

$$\frac{\partial\mathbf{A}}{\partial\rho_m}=\begin{bmatrix}\dfrac{\partial\mathbf{B}^{FE}}{\partial\rho_m} & \mathbf{0} & \mathbf{0} & \mathbf{0}\\ \mathbf{0} & \mathbf{0} & \mathbf{0} & \mathbf{0}\\ \mathbf{0} & \dfrac{\partial\mathbf{K}^{EFG}}{\partial\rho_m} & \mathbf{0} & \mathbf{0}\\ \mathbf{0} & \mathbf{0} & \mathbf{0} & \mathbf{0}\end{bmatrix} \tag{37}$$

where

$$\frac{\partial B^{FE}_{i,j}}{\partial\rho_m}=-\frac{1}{\rho_m^2}\int_{\Omega^m}\nabla\Phi_i^{FE}\cdot\nabla\Phi_j^{FE}\,d\Omega\qquad i,j=1,2,\ldots,N^{FE} \tag{38}$$

And

$$\frac{\partial K^{EFG}_{i,j}}{\partial\rho_m}=-\frac{1}{\rho_m^2}\int_{\Omega^m}\nabla\Phi_i^{EFG}\cdot\nabla\Phi_j^{EFG}\,d\Omega\quad i,j=1,2,\ldots,N^{EFG} \tag{39}$$

here Ω^m is the pixel region with respect to which the derivative is calculated. Obtaining $\partial\mathbf{b}/\partial\rho_m$ from (36) and considering $\mathbf{b}=\left[\hat{\mathbf{u}}^{FE}\quad\hat{\mathbf{u}}^{EFG}\quad\hat{\mathbf{U}}\quad\hat{\boldsymbol{\lambda}}\right]^T$, the derivative of coefficients $\partial\hat{\mathbf{U}}/\partial\rho_m$ is computed. Since the coefficients $\hat{\mathbf{U}}$ and potentials U_l on the electrodes are related by equation (16), the expression $\partial\mathbf{U}/\partial\rho_m$ is then obtained.

4. Evaluation and results

4.1. Forward problem simulations

In this section, the numerical results obtained from the FE, and hybrid FE-EFG methods are validated with an analytical solution for a homogeneous model. Moreover, a homogenous forward problem is solved and the proposed method is evaluated with experimental data. To quantify the accuracy of numerical results the following percent relative errors (RE) has been used:

$$\mathrm{RE}=\frac{\sqrt{(\mathbf{U}-\mathbf{E})(\mathbf{U}-\mathbf{E})^T}}{\sqrt{\mathbf{E}\,\mathbf{E}^T}}\times100\ \% \tag{40}$$

Where $\mathbf{U}$ is the electrodes voltage vector predicted by the forward model and $\mathbf{E}$ is the reference electrodes voltage vector.

4.1.1. Example I. Analytical solution and validation. In this example, a homogeneous circular model of radius 15cm and conductivity of $\sigma=1S/cm$ driven by $L=32$ symmetrical electrodes covering 50 percent of the surface.

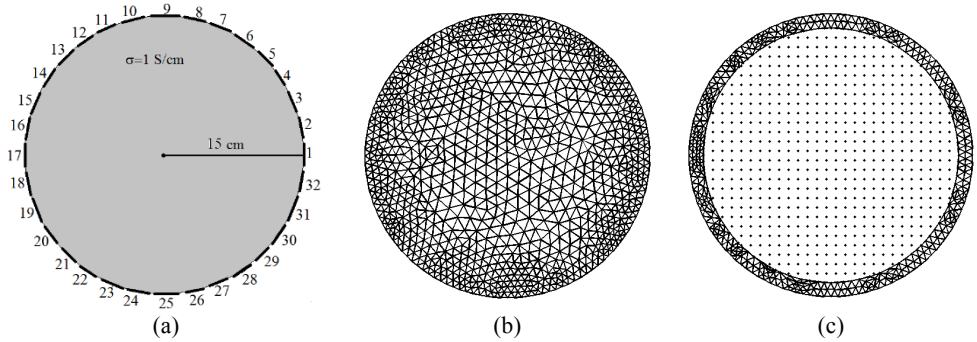

Figure 2. Example I. (a) Configuration of electrodes, (b) domain discretization with the FE method, and (c) domain discretization with the hybrid FE-EFG method

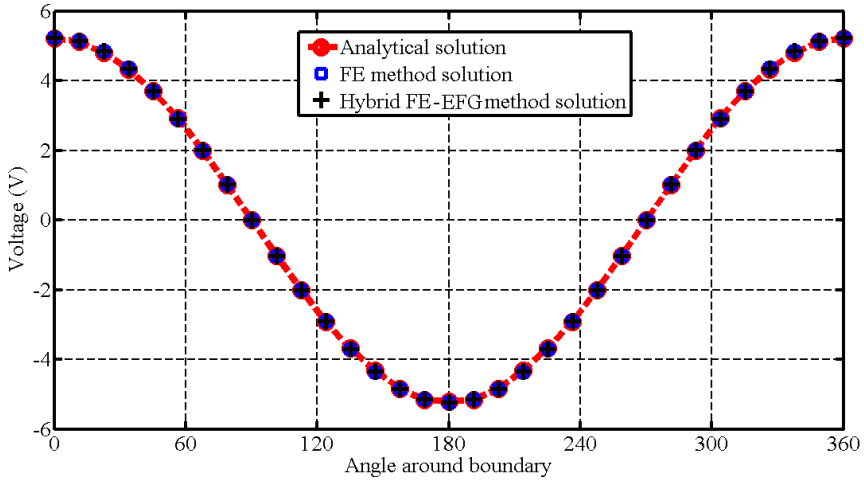

Figure 3. Example I. FE, hybrid FE-EFG, and analytical solutions for potential at electrodes

The electrodes have the same contact resistivity equal to $z_l = 0.22\,\Omega cm^2$. This example is like the model that used in the (Paulson *et al* 1992). The first optimal current pattern was applied, i.e. $I_l = \cos(2\pi l / L) \quad l = 1,2,\ldots,32$ (Cheney *et al* 1990). An analytical solution for a two dimensional disk has been reported in (Paulson *et al* 1992). The solution of the electrode voltages that are obtained from the two methods of solving forward model simulation are compared to the results obtained from the analytic solution. Figure 2 depicts configuration of electrodes and domain discretizations in the FE and hybrid FE-EFG methods.

The FE meshes in the pure FE method have 973 nodes and 1816 elements. In Figure 2(c), the radius of EFG region is 13.5 cm and the discretized FE domain includes 439 nodes and 652 elements. The discretized EFG domain has a uniform distribution and includes 658 nodes. There are 98 common nodes on the interface boundary Γ^{int}. Figure 3 depicts the FE and hybrid FE-EFG solutions together with analytical solution. For the FE method the RE being 0.63% and for the hybrid FE-EFG method the RE being 0.57%. There is a good agreement between numerical results and analytical solution.

4.1.2. Example II. An experimental homogenous phantom. In this example, a homogenous forward problem is solved and the proposed method is evaluated with experimental data. Figure 4 shows the experimental configuration that used in (Xu and Dong 2010). The problem has a circular cross section and has a diameter of 12.5 cm. The configuration includes 16 similar electrodes, evenly spaced on the problem boundary. Each electrode has 1 cm width, 0.1 cm thickness, and 3 cm height. An adjacent mode is adopted. 5 mA 60 kHz AC current is applied to electrode 1 and electrode 16 is grounded. The conductivity of the background is $\sigma = 662\ \mu S/cm$ and the electrodes have the same contact resistivity equal to $z_l = 57.8\,\Omega cm^2$ (Xu and Dong 2010).

The solution of the electrode voltages that are obtained from the two methods of solving forward model simulation are compared to the results obtained from the experimental results. Figure 5 depicts configuration of electrodes and domain discretizations in the FE and hybrid FE-EFG methods. The FE meshes in pure FE method have 653 nodes and 1208 elements. In hybrid method we consider two case for domain discretization. Case #1 is shown in Figure 7(b). In this case the nodes used in the pure FE method and the hybrid FE-EFG are identical. The discretized FE domain in hybrid method includes 310 nodes and 449 elements. These elements are the same as elements used in the pure FE method. The discretized EFG domain includes 418 nodes. These nodes are the same as nodes used in the pure FE method. There are 75 common nodes on the interface boundary Γ^{int}.

Case #2 is shown in Figure 5(b). In this case the radius of EFG region is 5.5 cm and the discretized FE domain includes 320 nodes and 442 elements. The discretized EFG domain has a uniform distribution and includes 418 nodes. There are 86 common nodes on the interface boundary Γ^{int}. Figure 6 depicts the FE and hybrid FE-EFG solutions together with experimental data. The RE in the pure FE method is 6.77% and the REs in the hybrid FE-EFG method are 5.02% and 4.65% for case #1 and case #2, respectively. There is a good agreement between numerical and experimental results. Case #2 manifests that the hybrid FE-EFG method can use a common boundary with an irregular shape such as a polygon.

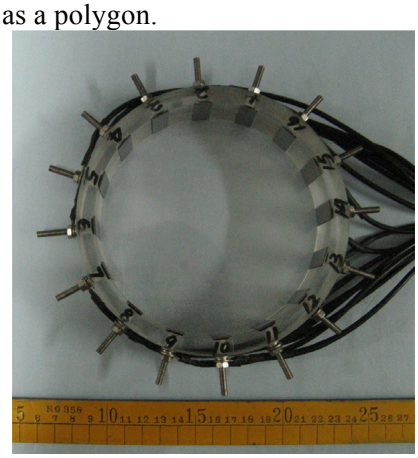

Figure 4. Example II. Experimental setup for EIT phantom (Xu and Dong 2010)

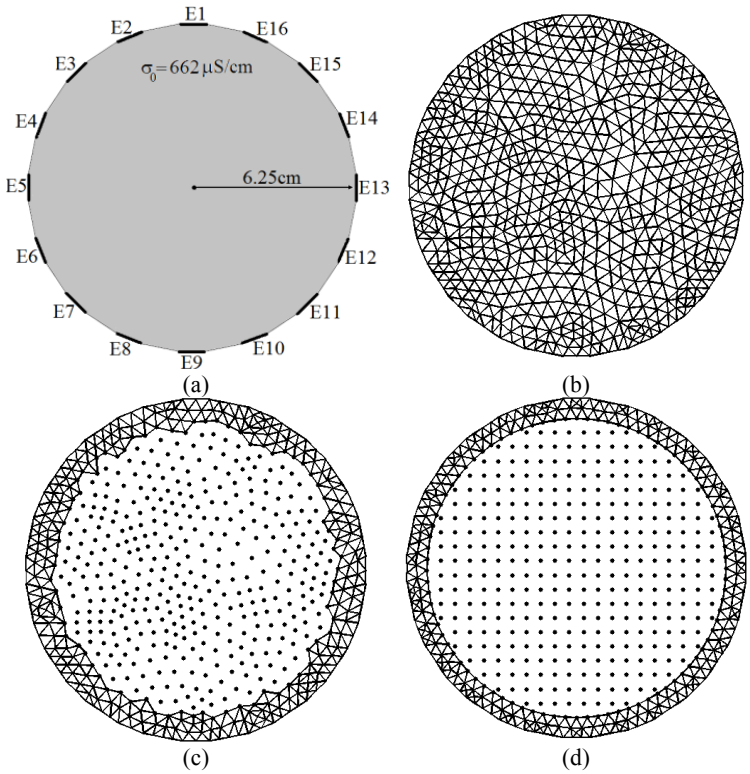

Figure 5. Example II. (a) Configuration of electrodes, domain discretizations with (b) the FE method, (c) the hybrid FE-EFG method and polygon common boundary, (d) the hybrid FE-EFG method and circular common boundary. Nodes are identical in parts (b) and (c).

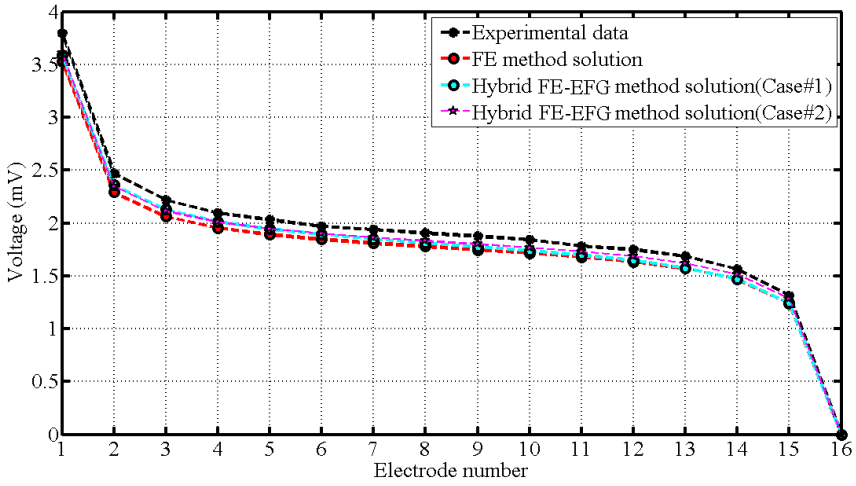

Figure 6. Example II. FE and Hybrid FE-EFG results of the potential at electrodes together with experimental data

4.2. Inverse problem simulations

4.2.1. Example III. A human chest phantom with experimental data. In order to demonstrate the efficiency of the hybrid FE-EFG method in the EIT inverse problem, the inverse problem in a biological phantom is investigated and comparisons between the hybrid FE-EFG and FE forward solvers in image reconstruction procedure are carried out. The boundary data set extracted from real measurements were acquired from the EIDORS website (http://eidors3d.sourceforge.net). The data sets were prepared for 2D imaging.

The data set was collected using ACT3 system which an adaptive neighbouring current injection method was applied (Isaacson *et al* 2004). This system corresponds to an experiment performed on a chest phantom containing agar heart and lungs suspended in a saline tank of radius 15 cm with 32 boundary electrodes of size 1.6 cm height and 2.5 cm width. The saline conductivity was 424 mS/m. The agar targets of the lungs had a conductivity of 240 mS/m, and the modeled heart was 750 mS/m. Trigonometric current patterns (Cheney *et al* 1990) are applied with maximum amplitude of 0.2 mA. Figure 7(a) shows an illustration of the experimental configuration of the phantom.

The images were reconstructed with 328 polygon pixels contributing to the Jacobian. These pixels that are similar to "Joshua tree" mesh introduced in (Cheney *et al* 1990) are shown in Figure 7(b). The initial distribution of resistivity is equal to resistivity of back ground and there is no information about internal subregion boundaries in the region of reconstruction.

The CEM is used as forward model and the FE and the hybrid FE-EFG methods are used as forward solvers.

To use the CEM, we need to know the contact impedance of the electrodes. Since actual values were not available to us, we assumed it to be constant and modelled the problem for different values of contact impedance. We observed that a range of contact impedance is acceptable. We chose a constant value equal to $z_l = 60\,\Omega cm^2$ for the contact impedance of all the electrodes in this paper. In practice, when this knowledge is not available, we could try to estimate the best mean square error for the contact impedance at each iteration of the inverse solution. In other words, we would solve the inverse problem to find both the conductivity values and the contact impedances (Babaeizadeh 2006). Figure 8 depicts the domain discritization used in the forward problem. The FE meshes in pure the FE method have 458 nodes and 800 elements. In hybrid method the radius of EFG region is 13.5 cm and the discretized FE domain includes 307 nodes and 453 elements. The discretized EFG domain has a uniform distribution and includes 209 nodes. There are 64 common nodes on the interface boundary Γ^{int}. Figure 9 shows the reconstructed images obtained with the regularization parameter $\mu = 0.5$ and after 4 iterations of Gauss–Newton method. The reconstructed conductivity based on the FE forward solver has a maximum value of 770 mS/m, found in the heart region. This constitutes a relative error of 2.66% for the heart region. The reconstructed images based on the hybrid FE-EFG forward solver have a maximum of 750 mS/m, found in the heart region, which corresponds to a relative error of 0.00%. The reconstructed conductivities based on the both FE and hybrid FE-EFG forward solvers have a minimum value of 200 mS/m, found in the lung region, which corresponds to a relative error of 16.66%. The overall size and position of the lungs and the agar heart appears accurate in both forward solvers.

Furthermore the image reconstruction for the homogeneous tank with the background conductivity of 424 mS/m for the saline is done with FE and hybrid FE-EFG forward solvers. Since the conductivity of pixels is constant for all pixels of a homogeneous phantom, the error analysis for conductivity of pixels can be down. The relative error

for reconstructed conductivity of pixels for the FE forward solver being 10.45% and for the hybrid FE-EFG forward solver being 10.05%. It indicates the image reconstruction based on the hybrid FE-EFG forward model is close to that of based on the FE forward model.

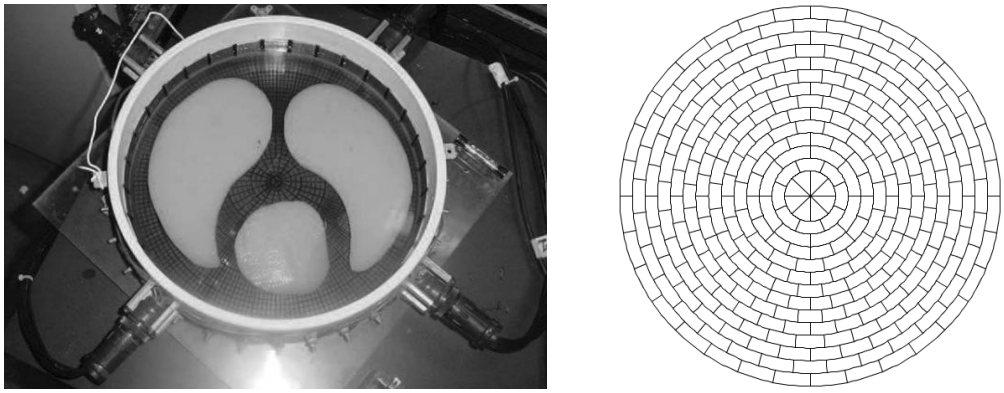

(a) (b)

Figure 7. Example III: a) The experimental chest phantom. © [2004] IEEE. Reprinted, with permission, from [Isaacson D, Mueller J L, Newell J C, and Siltanen S, Reconstructions of chest phantoms by the D-bar method for electrical impedance tomography *IEEE Trans. Med. Imaging*. 23 821-2], (b) 328 pixels used in the image reconstruction algorithm.

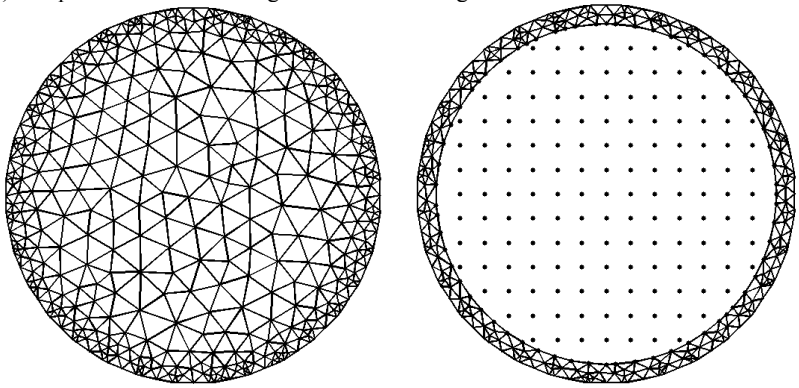

(a) (b)

Figure 8. Example III: (a) domain discretization for the FE forward solver, (b) domain discretization for the hybrid FE-EFG forward solver

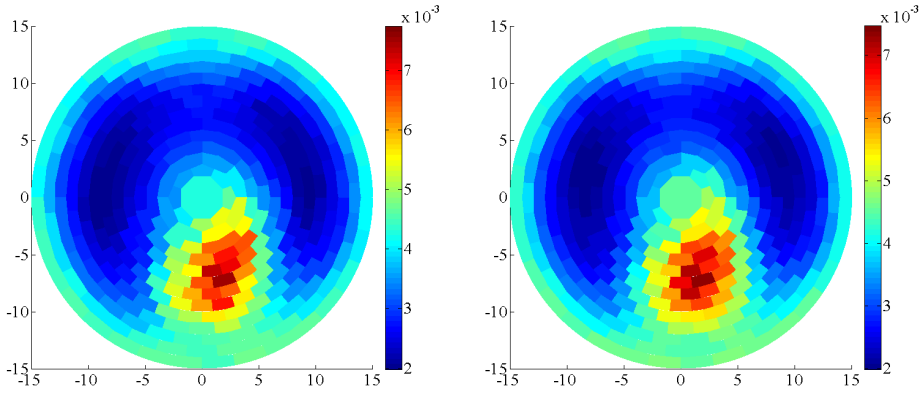

(a) (b)

Figure 9. Example III: image reconstruction with (a) FE forward solver, (b) hybrid FE-EFG forward

5. Conclusion

In this paper, a new approach for EIT image reconstruction was proposed, where the forward problem solution was modified. The hybrid FE-EFG method has been introduced for solving the EIT forward problem based on the CEM. The proposed method, which requires only a series of nodes in the meshfree region, eases the meshing task while keeping the accuracy of the traditional FE method. In the hybrid FE-EFG method, the EFG and FE regions are represented separately. Using the hybrid FE-EFG method, dependency of solution on FE mesh is reduced in some regions. The performance of the hybrid FE-EFG and FE methods have been validate using analytical solution and experimental data for 2D homogeneous problems. Image reconstruction for the human chest experimental phantom is accomplished by using the FE and hybrid FE-EFG forward solvers. The results give a general overview that the proposed method can introduce an effective numerical solution for EIT forward and

inverse problems. The future work will be continued on study of the capabilities of the proposed method in three dimensions which makes it more practical in medical applications.

Acknowledgments

The authors wish to thank David Stephenson, Jonathan Newell and David Isaacson for contributing experimental EIT data, and the administrators of the EIDORS project for facilitating the contribution of research experiences on electrical impedance tomography through the World Wide Web.

References

Babaeizadeh S, 2006 3-D Electrical impedance tomography for domains with piecewise constant conductivity Northeastern University Boston Publications, Massachusetts University C. Natural and Environmental Sciences 62

Bayford R H, Gibson A, Tizzard A A, Tidswell T and Holder D S 2001 Solving the forward problem in electrical impedance tomography for the human head using IDEAS (integrated design engineering analysis software), a finite element modelling tool *Physiol. Meas.***22** 55-64

Belytschko T, Lu Y Y and Gu L 1994 Element free Galerkin methods *Int. J. Numer. Meth. Eng*. **37** 229–56

Cheney M, Isaacson D and Newell J C 1990 NOSER: An algorithm for solving the inverse conductivity problem *Int. J. Imag. Syst., Technol.***2** 66–75

Cheney M, Isaacson D and Newell J C 1999 Electrical impedance tomography *SIAM Rev* **41** 85–101

Cheng K S, Isaacson D, Newell J C, and Gisser D G, 1989 Electrode models for electric current computed tomography *IEEE Trans. Biomed. Eng.* **36** 918–924

Cutrupi V, Ferraioli F, Formisano A, Martone R 2007 An approach to the electrical resistance tomography based on meshless methods *IEEE Trans. Mag.***43** 1717-20

Dolbow J and Belytschko T 1998 An introduction to programming the meshless element-free Galerkin method *Arch. Comput. Mech. Eng.***5** 207-42

Gang Hu, Minyou Ch, Wei He, and Jinqian ZH 2013 A novel forward problem solver based on meshfree method for electrical impedance tomography *Przeglad elektrotechniczny.* **43** 234-37

Ghaderi Daneshmand P and Jafari R 2013 A 3D hybrid BE–FE solution to the forward problem of electrical impedance tomography *Eng Anal Boundary Elem* **37** 757-64

Hadinia M and Jafari R 2015 An element-free Galerkin forward solver for the complete-electrode model in electrical impedance tomography *Flow Meas Instrum.* **45** 68-74

Hadinia M, Jafari R and Soleimani M 2015 A hybrid EFG-FE solution to the EIT forward problem based on the complete-electrode model *16th Int. Conf. on Biomedical Applications of electrical impedance tomography* (Switzerland) p 89

Hegen D 1996 Element-free Galerkin methods in combination with finite element approaches *Comput. Methods Appl. Mech. Eng.* **135** 143-66

Herault C and Markcha1 Y 1999 Boundary and interface conditions in meshless methods *IEEE Trans. Mag.* **35** 1450-53

Isaacson D, Mueller J L, Newell J C, and Siltanen S 2004 Reconstructions of chest phantoms by the D-bar method for electrical impedance tomography *IEEE Trans.* Med. *Imaging.* **23** 821-28

Muria T and Kagwa Y 1985 Electrical impedance computed tomography based on a finite element model *IEEE Trans. Biomed. Eng.* **32** 177-84

Paulson K S, Breckon W R and Pidcock M K, 1992 Electrode modelling in Electrical Impedance Tomography, *SIAM J. Appl. Math.* **52** 1012–1022

Rezajoo S and Hossein-zadeh G A 2010 Reconstruction convergence and speed enhancement in electrical impedance tomography for domains with known internal boundaries *Physiol. Meas.***31** 1499-516

Saulnier G J, Blue R S, Newell J C, Isaacson D and Edic P M 2001 Electrical impedance tomography *IEEE* Signal Processing Mag **18** 31-43

Somersalo E, Cheney M, and Isaacson D, 1992 Existence and uniqueness for electrode models for electric current computed tomography *SIAM J. Appl. Math.* **52** 1023–1040

Šterk M, and Trobec R 2008 Meshless solution of a diffusion equation with parameter optimization and error analysis*Eng Anal Boundary Elem*. **32** 567-77

Vauhkonen M, 1997 Electrical impedance tomography and prior information Kuopio University Publications C. Natural and Environmental Sciences 62

Vauhkonen P J, Vauhkonen M, Savolainen T, and Kaipio J P, 1999 Three-dimensional electrical impedance tomography based on the complete electrode model *IEEE Trans. Biomed. Eng.* **46** 1150-1160

Xu Y, Dong F, 2010 Galerkin boundary element method for the forward problem of ERT. *Flow Meas Instrum* **21** 172-17.

Yorkey T, Webster J G and Tompkins W J 1987 Comparing reconstruction algorithm for electrical impedance tomography *IEEE Trans. Biomed. Eng.***34** 843-52

Yousefi M R, Jafari R and Abrishami-Moghaddam H 2013 A Combined Wavelet-Based Mesh-Free Method for Solving the Forward Problem in Electrical Impedance Tomography *IEEE Trans. Instrum. Meas* **62** 2629-38

Yousefi M R, Jafari R and Abrishami-Moghaddam H 2014 Imposing boundary and interface conditions in multi-resolution wavelet Galerkin method for numerical solution of Helmholtz problems *Comput. Methods Appl. Mech*. **276** 67-94